

Probing muonic force with periastron advance in binary pulsar systems

Zuwei Liu¹ and Zi-Wei Tang¹

¹*Department of Physics, Nanjing University, Nanjing 210093, China*

Pulsars, highly magnetized, rotating neutron stars, can have significant muon abundances in their dense cores, making them promising environments to probe ultralight mediators coupled to muons. The precise measurement of periastron advance in binary pulsar systems provides a sensitive probe of such long-range forces. In this work, we study the periastron advance constraints from binary pulsar systems on the ultralight muonic mediators. We compute the muon number fraction in neutron stars, by properly taking into account the suppression effect of the long-range muonic force. We find that the periastron advance constraints impose the most stringent constraints on ultralight muonic mediators in the mass range of $\simeq (10^{-17}, 2 \times 10^{-15})$ eV, probing muonic couplings as small as $\mathcal{O}(10^{-21})$, which surpass the limits from LIGO/Virgo gravitational wave measurements, by about an order of magnitude.

I. INTRODUCTION

The exploration of new long-range forces has spanned a broad range of distances and coupling strengths [1]. The long-range forces that act on neutrons, protons, or electrons are tightly constrained by the experimental tests of the weak equivalence principle (WEP) [2–8]. On the other hand, the long-range forces that act on muons remain largely unconstrained, because muons are rare in most WEP experiments. One of the ways to search for muonic forces is to study their effects on the inspiral dynamics of binary systems involving neutron stars (NS) that have significant muon fractions [9]. Constraints on muonic forces from such systems have been carried out through gravitational wave signals [10, 11] and orbital decays [10, 12].

In this work, we use periastron advance of the binary pulsar system to search for ultralight mediators coupled to muons. The periastron advance for many binary pulsar systems has been measured with great precision [13–18]. Recently, tests of general relativity (GR) and beyond [1, 19–22], as well as searches for beyond-the-Standard-Model (BSM) physics [23–25] using the precise pulsar periastron advance measurements have been carried out. Because the periastron advance induced by muonic forces is strongly dependent on the muon abundance in the neutron star core, it is of great importance to properly take into account the effects of the muonic Yukawa potential, which can significantly decrease the muon abundance. This suppression arises from the potential energy associated with the muonic force, which raises the energy needed to produce muons in the NS core, thereby reducing the muon fraction. Although such an effect has been mentioned in Ref. [10], it has not been quantitatively analyzed for muon abundances in neutron star cores before. We find that the suppression of NS muon fraction due to the muonic force cannot be neglected for scalar-muon coupling $g_{\phi\mu} \gtrsim 10^{-19}$. For example, the muon fraction decreases to one-third of its Standard Model (SM) value for the $g_{\phi\mu} = 10^{-18}$ case.

By carefully taking into account the effects on the muon fraction from the long-range force, we find that

the pulsar periastron advance provides the most stringent constraints and is sensitive to the muonic force for the mediator mass between 10^{-18} and $\mathcal{O}(10^{-14})$ eV. In this parameter space, the muonic force was previously constrained by gravitational wave signal from the NS-NS merger event detected by the LIGO/Virgo collaboration [10, 26]. We find that the periastron advance of binary pulsars provides the most stringent constraints on the mediator mass range $\simeq (10^{-17}, 2 \times 10^{-15})$ eV, surpassing the GW170817 constraints by up to one order of magnitude.

The rest of the paper is organized as follows. In section II we analyze the pulsar periastron advance induced by ultralight mediators coupled to muons. In section III we compute the muon fraction, by properly taking into account the effects of the long-range Yukawa potential. In section IV, we compute the constraints on scalar-muon couplings from the orbital decay measurements of binary pulsars. In section V we present the pulsar periastron advance constraints and the orbital decay constraints on muonic couplings. We summarize our findings in section VI. Some detailed analyses are given in appendices, including the neutron star structure and particle number densities in appendix A, and expressions of the radiation power in appendix B.

II. NEW MUONIC FORCE AND PERIASTRON ADVANCE

In this section we consider a new muonic force between the pulsar and its companion NS in binary systems and study its effects on the periastron advance.

A. New ultralight scalar

We consider an ultralight scalar ϕ that couples to muons via the following interaction Lagrangian

$$\mathcal{L}_{\text{int}} \supset g_{\phi\mu} \phi \bar{\mu} \mu, \quad (1)$$

where $g_{\phi\mu}$ is the dimensionless coupling constant. We note that our analysis of the periastron advance for the

scalar mediator is readily applicable to the vector mediator.

Because NS can have a substantial muon fraction [9, 27], the new muonic ultralight mediator ϕ then results in a long-range potential for muons inside NSs

$$V(R) = \frac{Q}{4\pi R} e^{-R/\lambda}, \quad (2)$$

where $Q = g_{\phi\mu} N_\mu$ is the muonic charge of the NS with N_μ being the total muon number inside the NS, R is the radial distance from the center of the NS, and $\lambda = 1/m_\phi$ is the Compton wavelength of the light mediator with m_ϕ being the mediator mass. Thus, in this case, muons experience an additional muonic Yukawa potential in addition to the gravitational potential. We compute the muon number of NSs in section III. We find that the total muon number is $N_\mu \simeq 3 \times 10^{55}$ for a typical NS with a mass of $m_{\text{NS}} = 1.4 M_\odot$.

For a binary system of a pulsar and an NS, the total force between the two orbiting stars can then be written as follows

$$F(R) = \frac{Gm_1m_2}{R^2} \left[1 - \alpha e^{-\frac{R}{\lambda}} \left(1 + \frac{R}{\lambda} \right) \right], \quad (3)$$

where G is the gravitational constant, R is the distance between the two stars, m_1 and m_2 are the masses of the pulsar and its companion NS, respectively, and

$$\alpha \equiv \frac{Q_1 Q_2}{4\pi G m_1 m_2}, \quad (4)$$

is the dimensionless parameter characterizing the relative strength of the muonic force with Q_1 and Q_2 being the muonic charges of the pulsar and its companion NS, respectively. Note that if λ is comparable to or larger than the semi-major axis of the binary system, the new muonic long-range force in Eq. (3) is not exponentially suppressed and can thus be quite substantial. For instance, the Hulse-Taylor binary pulsar, PSR B1913+16 [28], has a semi-major axis of $a \simeq 2 \times 10^6$ km, which can be inferred from its orbital period P_b [14] via the Kepler's third law $a = [GMP_b^2/(4\pi^2)]^{1/3}$. Thus, to generate a substantial muonic force between the Hulse-Taylor pulsar and its companion (NS), the mass of the scalar is $\lesssim 10^{-16}$ eV.

B. Periastron advance

The new muonic force provides a new contribution to the periastron advance of the binary systems. We denote the position vectors of two orbiting stars in the binary system with \vec{R}_1 and \vec{R}_2 , respectively. In the center of mass (CM) frame of the binary system, the equation of motion is [29]

$$\vec{a} = -\frac{GM}{R^2} \vec{n} + \delta\vec{a}, \quad (5)$$

where $M = m_1 + m_2$ is the total mass of the binary system, $\vec{R} = \vec{R}_1 - \vec{R}_2$, $\vec{a} \equiv d^2\vec{R}/dt^2$, $\vec{n} = \vec{R}/R$, and $\delta\vec{a}$ is the acceleration beyond the Newtonian case. Here, $\delta\vec{a}$ can be induced both by GR and by new physics:

$$\delta\vec{a} = \vec{a}_{\text{PN}} + \vec{a}_\phi, \quad (6)$$

where \vec{a}_{PN} is the post-Newtonian (PN) contribution, and

$$\vec{a}_\phi = \frac{GM}{R^2} \alpha e^{-\frac{R}{\lambda}} \left(1 + \frac{R}{\lambda} \right) \vec{n}, \quad (7)$$

is the new physics contribution. The 1PN contribution is [29, 30]

$$\vec{a}_{\text{PN}} = -\frac{GM}{R^2} \left\{ \left[(1 + 3\eta)v^2 - \frac{3}{2}\eta\dot{R}^2 - 2(2 + \eta)\frac{GM}{R} \right] \vec{n} - \left[2(2 - \eta)\dot{R} \right] \vec{v} \right\}, \quad (8)$$

where $\eta = m_1 m_2 / M^2$, $\vec{v} = d\vec{R}/dt$ is the relative velocity, and $v = |\vec{v}|$.

In the presence of $\delta\vec{a}$, the longitude of the periastron, denoted by ω , advances as the stars orbit each other, known as the periastron advance. After the pulsar completes one orbit with the period P_b , the change in the angle ω is

$$\Delta\omega = \Delta\omega_\phi + \Delta\omega_{\text{PN}}, \quad (9)$$

where [29, 31]

$$\Delta\omega_\phi = \int_0^{2\pi} df \left(\frac{d\omega}{df} \right)_\phi, \quad (10)$$

$$\left(\frac{d\omega}{df} \right)_\phi = -\frac{a^2(1-e^2)^2}{GM e} \frac{\cos f}{(1+e\cos f)^2} (\vec{a}_\phi \cdot \vec{n}),$$

where f is the true anomaly for the eccentric orbit, $a = [GM(P_b/2\pi)^2]^{1/3}$ is the semi-major axis of the orbit, and e is the orbital eccentricity. The 1PN contribution to the periastron advance is [29]

$$\Delta\omega_{\text{1PN}} = \frac{6\pi GM}{a(1-e^2)}. \quad (11)$$

The 2PN contribution to the periastron advance is [13, 32]

$$\Delta\omega_{\text{2PN}} = \frac{6\pi}{1-e^2} f_O \beta_O^4,$$

$$\beta_O = \left(\frac{2\pi GM}{P_b} \right)^{1/3},$$

$$f_O = \frac{1}{1-e^2} \left[\frac{39}{4} \left(\frac{m_1}{M} \right)^2 + \frac{15m_1m_2}{M^2} + \frac{27}{4} \left(\frac{m_2}{M} \right)^2 \right]$$

$$- \left[\frac{13}{4} \left(\frac{m_1}{M} \right)^2 + \frac{13m_1m_2}{3M^2} + \frac{1}{4} \left(\frac{m_2}{M} \right)^2 \right]. \quad (12)$$

PSR	$\dot{\omega}_{1\text{PN}}$ (deg/yr)	$\dot{\omega}_{2\text{PN}}$ (deg/yr)	$\dot{\omega}_{3\text{PN}}$ (deg/yr)	$\dot{\omega}_{\text{data}}$ (deg/yr)	m_1 (M_\odot)	m_2 (M_\odot)
J0737-3039A [13]	16.899139	0.000440	1.8×10^{-8}	16.899323(13)	1.338	1.249
B1916+13 [14]	4.226226	0.000098	3.2×10^{-9}	4.226585(4)	1.438	1.390
J1906+0746 [15]	7.5836	0.0001	4.3×10^{-9}	7.5841(5)	1.291	1.322
J1756-2251 [16]	2.58306	0.00003	6.5×10^{-10}	2.58240(4)	1.341	1.230
B2127+11C [17]	4.4635	0.0001	4.2×10^{-9}	4.4644(1)	1.358	1.354
B1534+12 [18]	1.7560312	0.0000199	3.6×10^{-10}	1.7557950(19)	1.333	1.346

TABLE I. The observed periastron advance rate, $\dot{\omega}_{\text{data}}$, and the PN contributions for six different pulsar systems. The 1PN, 2PN, and 3PN contributions are computed via Eq. (11), Eq. (12), and equation (539b) of Ref. [30], respectively. The numbers in the parentheses indicate the 1σ uncertainties of $\dot{\omega}_{\text{data}}$. The masses (rounded to four significant figures) shown in the last two columns are from the references in the first column, and are used to compute the PN contributions in this table.

PSR	γ (ms)	s	\dot{P}_b^{int} (10^{-12})	m_1 (M_\odot)	m_2 (M_\odot)
J0737-3039A [13]	-	0.999936(9, 10)	-1.247782(79)	(1.33801, 1.33830)	(1.24878, 1.24894)
B1916+13 [14]	4.307(4)	-	-2.398(0.004)	(1.430, 1.442)	(1.387, 1.393)
J1906+0746 [15]	0.470(5)	-	0.55(3)	(1.14, 1.41)	(1.26, 1.37)
J1756-2251 [16]	1.148(9)	-	-0.234(6, 9)	(1.33, 1.51)	(1.23, 1.30)
B2127+11C [17]	4.78(4)	-	-3.95(13)	(1.28, 1.46)	(1.32, 1.40)
B1534+12 [18]	2.0708(5)	0.9772(16)	-	(1.32, 1.40)	(1.34, 1.37)

TABLE II. The masses for the pulsar (m_1) and its companion NS (m_2), along with the PK parameters used to derive the masses, for six binary systems. The measured values of x are 1.415028603(92) s for PSR J0737-3039A [13], and 3.7294636(6) for PSR B1534+12 [18]. For the PK parameters, numbers in parentheses denote the 1σ uncertainties; for the masses, numbers in parentheses denote the 2σ uncertainties.

We neglect higher order PN contributions, as they are much smaller than the precision of the binary pulsar systems considered in our analysis, as shown in Table I.

The periastron advance rate is

$$\dot{\omega} = \frac{\Delta\omega}{P_b} = \frac{\Delta\omega_{\text{PN}}(m_1, m_2) + \Delta\omega_\phi(m_1, m_2, \alpha)}{P_b}, \quad (13)$$

where $\Delta\omega_{\text{PN}}$ is given in Eqs. (11-12), and $\Delta\omega_\phi$ is given in Eq. (10).

C. Binary masses

To compute the periastron advance rate, one has to determine the masses of the pulsar and its companion. In the DD timing model [33] used for the data analysis of the binary pulsars [13–18], the masses of the binary stars are derived from the measured post-Keplerian (PK) parameters [34].¹ In our analysis we consider the following four PK parameters for the mass determination of the binary pulsar systems²:

- The periastron advance rate $\dot{\omega}$.
- The amplitude of the gravitational redshift - time dilation term γ [14]:

$$\gamma = e \left(\frac{P_b}{2\pi} \right)^{1/3} T_\odot^{2/3} M^{-4/3} m_2 (m_1 + 2m_2), \quad (14)$$

where $T_\odot \equiv GM_\odot$ [14].

- The shape of the Shapiro delay s [13]:

$$s = \sin i = \frac{2\pi x M}{P_b \beta_O m_2} \left[1 + \left(3 - \frac{m_1 m_2}{3M^2} \right) \beta_O^2 \right], \quad (15)$$

where $\beta_O = (2\pi GM/P_b)^{1/3}$, and x is the projected semi-major axis.

- The intrinsic orbital decay rate \dot{P}_b^{int} [14]:

$$\dot{P}_b^{\text{int}} = -\frac{192\pi}{5} \left(\frac{P_b}{2\pi} \right)^{-5/3} \left(1 + \frac{73}{24} e^2 + \frac{37}{96} e^4 \right) \times (1 - e^2)^{-7/2} T_\odot^{5/3} m_2 m_1 M^{-1/3}, \quad (16)$$

which accounts for the quadrupole gravitational radiation. Note that \dot{P}_b^{int} is obtained from the observed orbital decay by removing external contributions, such as the difference in the galactic gravitational accelerations between the barycenter of the solar system and the binary pulsar system [13]. For

¹ For example, the masses of PSR B1916+13 can be determined by $\{\dot{\omega}, \dot{P}_b^{\text{int}}, \gamma, s, r\}$, as shown in figure 4 of [14], where r is the range of the Shapiro delay [34].

² A detailed description of various PK parameters can be found in Ref. [34].

PSR J0737-3039, we also consider the higher-order contributions to \dot{P}_b^{int} due to the 3.5PN contribution in the equations of motion, which is -1.75×10^{-17} [13].

For the six binary pulsars we considered, $\dot{\omega}$ is the PK parameter that leads to the best-measured masses in GR [13–18]; the masses obtained using $\dot{\omega}$ are shown in Table I. In our analysis, however, we do not use $\dot{\omega}$ to determine the masses, since we use $\dot{\omega}$ to compute constraints on new physics. Instead we use γ , s , and \dot{P}_b^{int} to determine the masses; we select two of the three PK parameters that lead to the masses that have the smallest uncertainties. The obtained masses and the PK parameters used to compute the masses are shown in Table II. We find that the masses in Table II are consistent with the masses in Table I.

D. Binary pulsars

Table I shows the observed periastron advance rate and the 1PN, 2PN and 3PN contributions for six different binary pulsar systems. The 2PN contribution is necessary for some of the binary pulsar systems in our analysis, since they have highly precise timing data. For example, the periastron advance rate of the double pulsar system PSR J0737-3039A has been measured with an uncertainty of 7.7×10^{-7} times its measured value. Note that for PSR J0737-3039A, we also incorporate the spin-orbit coupling effect, which is $-4.83_{-0.35}^{+0.29} \times 10^{-4}$ deg/yr [13]. As shown in Table I, the 3PN corrections are smaller than the experimental uncertainties and thus can be neglected.

To compute the constraints, we use Eq. (13), where the observed values of $\dot{\omega}$ from the pulsar-NS binary systems are given in Table I, and the components masses are given in Table II. Fig. 1 shows the upper bound at the 2σ level on the parameter α . Among the six binary systems we consider in Table I, PSR J0737-3039A has the most accurate timing measurements, leading to the most stringent constraints on α .

III. MUON FRACTION OF NEUTRON STAR

In this section we further compute the constraints on the muonic coupling $g_{\phi\mu}$ by using the constraints on α shown in Fig. 1. To do so, we compute the charge-to-mass ratio Q/m of an NS via

$$\frac{Q}{m} = \frac{g_{\phi\mu}}{m_n} \frac{N_\mu}{N_n} \equiv \frac{g_{\phi\mu}}{m_n} Y_\mu, \quad (17)$$

where N_μ and N_n are the total number of muons and nucleons inside the NS, respectively, $m_n \simeq 940$ MeV is the mass of the neutron, and $Y_\mu \equiv N_\mu/N_n$ is the muon fraction. In our analysis for the NS, we use the equation-of-state (EoS) model BSk24 [27], which is the EoS model

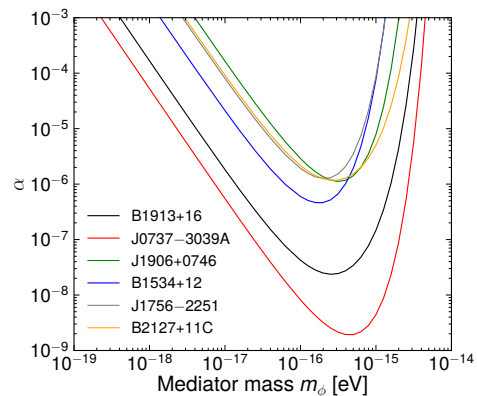


FIG. 1. The 2σ bounds on α from the periastron advance of binary pulsar systems.

in the analysis of the binary merger event GW230529 [35]. The nucleon number inside an NS is given by $N_n = m_{\text{NS}}/(e_{\text{eq}} + m_n)$, where e_{eq} is the energy per nucleon without the nucleon mass [27], and we have neglected the mass difference between neutron and proton. Note that the pulsars in our analysis have $e_{\text{eq}} \ll m_n$; for instance, e_{eq} of PSR J0737-3039A is in the range of $\sim (62.7, -9.0)$ MeV from the center to the outer crust. Thus, we further neglect e_{eq} and use $N_n \simeq m_{\text{NS}}/m_n$ to determine the total nucleon number.

We next compute the muon fraction Y_μ inside an NS in the presence of an ultralight mediator ϕ . For that purpose, one has to account for the effects from the Yukawa potential induced by the ultralight mediator on the muon fraction. Although such effects have been mentioned in Ref. [10], their significance has been somewhat overlooked and thus neglected. We find that such effects are significant in the parameter space of interest so that they must be taken into account properly in the calculation.

Neutron stars are primarily composed of neutrons, protons, electrons, and muons, known as the $npe\mu$ matter [9]. Muons can be produced in the NS core if the Fermi energy of electrons exceeds the rest mass of the muon, $m_\mu = 105.65$ MeV. Because the Fermi energy of electrons can be as high as ~ 122 MeV in the NS core [9], a substantial muon abundance is expected in the NS core.

If the $npe\mu$ matter is at equilibrium, the chemical potential of the muon is equal to the chemical potential of the electron [9, 27]:

$$\mu_e = \mu_\mu. \quad (18)$$

The chemical potential of the electron is given by

$$\mu_e(r) = \sqrt{m_e^2 + [3\pi^2 n_e(r)]^{2/3}}, \quad (19)$$

where $n_e(r)$ is the number density of the electron at the radial coordinate r of the NS. The chemical potential of the muon is given by

$$\mu_\mu(r) = \sqrt{m_\mu^2 + [3\pi^2 n_\mu(r)]^{2/3}} + V_\phi(r), \quad (20)$$

where $n_\mu(r)$ is the muon number density at the radial coordinate r of the NS, and $V_\phi(r)$ is the potential energy due to the ultralight mediator ϕ . In the parameter space of interest we have ³

$$V_\phi(r) = g_{\phi\mu}^2 \int_r^\infty \frac{dr'}{r'^2} \int_0^{r'} dr'' r''^2 n_\mu(r''). \quad (21)$$

Here we have approximated the Yukawa potential induced by the ultralight mediator ϕ with the Coulomb potential. This approximation is justified because the Compton wavelength probed by the periastron advance measurement is comparable to the separation between the two neutron stars in the binary system, which is typically much larger than the radius of an NS. For example, the separation between the two NSs in PSR J0737-3039 is $\sim 10^6$ km, whereas the radii of the NSs are ~ 10 km. Therefore, the Coulomb potential provides a reasonable approximation of the Yukawa potential when computing the muon distributions within the NS. We provide a detailed derivation of Eqs. (18-20), and the electron density profile $n_e(r)$ in Appendix A.

Because μ_μ increases with $g_{\phi\mu}^2$, the amount of energy required to produce muons becomes large in the parameter region where the coupling constant $g_{\phi\mu}$ is large. This then leads to a suppression on the muon fraction in the large coupling region.

To determine the profile of the muon number density, we employ an iterative procedure to solve Eq. (20) such that the muon profile at the i -th iteration is given by

$$n_{\mu,i}(r) = \frac{1}{3\pi^2} \left\{ \left[\mu_e(r) - g_{\phi\mu}^2 \int_r^\infty dr' \frac{1}{r'^2} \times \int_0^{r'} dr'' r''^2 n_{\mu,i-1}(r'') \right]^2 - m_\mu^2 \right\}^{\frac{3}{2}}, \quad (22)$$

where $n_{\mu,i-1}(r)$ is the muon profile at $(i-1)$ -th iteration. For $n_{\mu,0}(r)$ in the first iteration, we use the profile obtained with $g_{\phi\mu} = 0$ such that

$$m_e^2 + [3\pi^2 n_e(r)]^{2/3} = m_\mu^2 + [3\pi^2 n_{\mu,0}(r)]^{2/3}. \quad (23)$$

The iteration is terminated at

$$\delta\mu(r) \equiv \left| \frac{\mu_e(r) - \mu_\mu(r)}{\mu_e(r)} \right| \leq 1\%, \quad (24)$$

for the r values of interest. We consider the range between $r = 0.1$ km and $r = r_0$ where r_0 is given by

$$\sqrt{m_e^2 + [3\pi^2 n_e(r_0)]^{2/3}} = m_\mu. \quad (25)$$

We then sample points evenly spaced on a logarithmic scale within the range. Note that muon production is

negligible in the region of $r > r_0$, where the electron Fermi energy drops below the muon rest mass. Fig. 2 shows the muon number density profile for the case where $g_{\phi\mu} = 10^{-18}$ and the NS mass is $1.4 M_\odot$. In this case, we find that $\delta\mu(r) < 0.2\%$ for $r \in (0.1 \text{ km}, r_0)$, where $r_0 \simeq 11.2$ km. As shown in Fig. 2, the muon number density in the $g_{\phi\mu} = 10^{-18}$ case is approximately three times smaller than in the $g_{\phi\mu} = 0$ case.

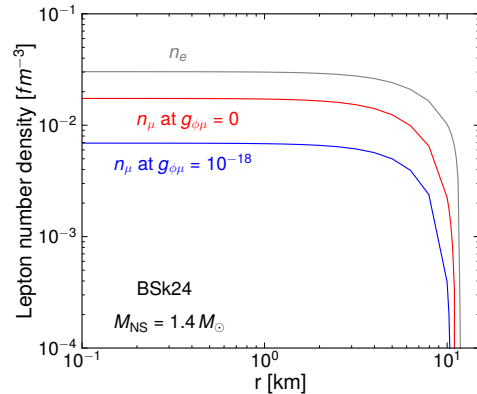


FIG. 2. Lepton number density as a function of the radial distance r for an NS with a mass of $m = 1.4 M_\odot$, where the EoS is BSk24 [27]. The muon number density profiles are shown for the $g_{\phi\mu} = 10^{-18}$ case (blue) and for the $g_{\phi\mu} = 0$ (red). Also shown is the electron number density profile (gray).

We note that the iterative method in our analysis works well in the small coupling regime, specifically for $g_{\phi\mu} \lesssim 10^{-18}$. However, in the large coupling regime of $g_{\phi\mu} \gtrsim 10^{-18}$, our iterative method fails to find solutions for n_μ . This could be due to the fact that as $g_{\phi\mu}$ increases, the muonic potential term in Eq. (22) becomes significant so that it disrupts the convergence of the iterative process. Consequently, we restrict our analysis to $g_{\phi\mu} \leq 10^{-18}$ and leave the investigation of larger couplings for future work.

We then calculate the muon number fraction with the integral

$$Y_\mu = \frac{\int_0^{R_{\text{NS}}} r^2 n_\mu(r) dr}{\int_0^{R_{\text{NS}}} r^2 n(r) dr}, \quad (26)$$

where $n(r)$ is the nucleon number density inside the NS, and R_{NS} is the radius of the NS. The calculations for $n(r)$ and R_{NS} are given in Appendix A.

Fig. 3 shows the muon number fraction Y_μ as a function of the coupling $g_{\phi\mu}$. We find that the new contribution to the muon fraction due to the muonic potential induced by ϕ can no longer be neglected for $g_{\phi\mu} \gtrsim 10^{-19}$.

IV. PULSAR ORBITAL DECAY CONSTRAINTS

In this section we obtain the pulsar orbital decay constraints on muonic couplings. We attribute the difference

³ Our analysis on V_ϕ differs from Ref. [10] (equation 2 therein) by an overall sign.

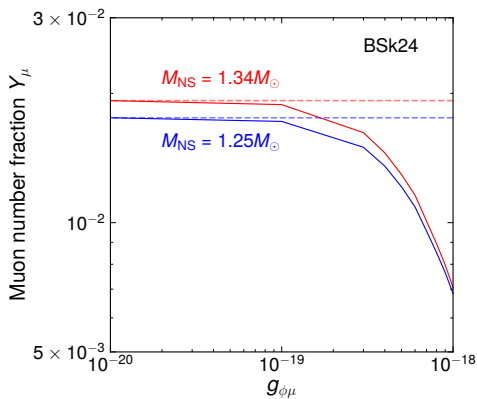


FIG. 3. The muon number fraction $Y_\mu \equiv N_\mu/N_n$ as a function of the coupling $g_{\phi\mu}$ for NSs with masses of $1.34 M_\odot$ (red-solid) and $1.25 M_\odot$ (blue-solid). The Y_μ values in the $g_{\phi\mu} = 0$ cases are shown as dashed lines.

between the intrinsic orbital decay with the predictions of general relativity (GR) to dipole radiation from the ultralight mediator. To obtain constraints on new physics, we use [36]

$$\frac{\langle \dot{E} \rangle_{S,V}(\gamma)}{\langle \dot{E} \rangle_G} = 1 - \frac{\dot{P}_b^{\text{GR}}}{\dot{P}_b^{\text{int}}}, \quad (27)$$

where \dot{P}_b^{GR} is the GR-predicted orbital decay, \dot{P}_b^{int} is the intrinsic orbital decay, and $\langle \dot{E} \rangle_{S,V}$ and $\langle \dot{E} \rangle_G$ are the time-averaged radiation powers, with S , V , G denoting the scalar mediator, vector mediator, and gravity, respectively. Note that $\langle \dot{E} \rangle_{S,V}$ is a function of $\gamma = [(Q/m)_1 - (Q/m)_2]^2 / (4\pi G)$, which is the strength of the dipole radiation. The expressions for the radiation powers are given in Appendix B. Fig. 4 shows constraints (at the 2σ level) on γ for both the scalar and vector mediators, from the binary pulsar systems in Table III. The strongest bounds come from the latest observation of the double pulsar system PSR J0737-3039A [13].

To compute constraints on the scalar/vector-muon coupling g , we use

$$\begin{aligned} \gamma &= \frac{1}{4\pi G} \left[\left(\frac{Q}{m} \right)_1 - \left(\frac{Q}{m} \right)_2 \right]^2 \\ &= \frac{g^2}{4\pi G m_n^2} (Y_{\mu,1} - Y_{\mu,2})^2, \end{aligned} \quad (28)$$

where $Y_{\mu,i}$ are the muon fraction of the NS or white dwarf (WD) with $i = 1, 2$ denoting the pulsar and its companion. We use Eq. (26) to compute Y_μ for the NS; for white dwarfs, we assume $Y_\mu = 0$ [37].

V. RESULTS

Fig. 5 shows the constraints on the scalar-muon coupling $g_{\phi\mu}$ from the periastron advance of PSR J0737-3039A and from the orbital decay measurements of the

binary pulsar systems given in Table III. The constraints from NS-WD binaries are generally more stringent than those from NS-NS binaries, except for the double pulsar system PSR J0737-3039A. That NS-WD binaries provide better constraints is primarily due to the vanishing muon fraction in WDs, which leads to a typically large $(Y_{\mu,1} - Y_{\mu,2})^2$ factor in Eq. (28). The most stringent constraint from the double pulsar system PSR J0737-3039A, is primarily due to the high precision measurements of the orbital decay.

We compare our results with the GW170817 constraints given in Ref. [10], which are analyzed for the $L_\mu - L_\tau$ gauged boson. We obtain the GW170817 limits on $g_{\phi\mu}$ (due to dipole radiation) by rescaling the ones given in Ref. [10] by a factor of $\sqrt{2}$, since the radiation power of the scalar mediator is a factor of 2 smaller than that of the vector mediator [36], leading to a weaker constraint on γ by a factor of 2. The GW170817 constraints depend on the muon abundance, which in turn depends on the EoS. Ref. [10] analyzed the GW170817 limits using four different EoS from Ref. [27], including BSk22, BSk24, BSk25, and BSk26. The envelope of these four cases is shown in Fig. 5. Note that the BSk22 (BSk26) EoS predicts the highest (lowest) muon abundance [10], and the muon abundance predicted by the BSk24 EoS lies in between.

As shown in Fig. 5, the pulsar orbital decay constraints are compatible with the GW170817 constraints [10] for $m_\phi \lesssim 10^{-19}$ eV. The constraints from the pulsar periastron advance are the strongest for the mediator mass range of $m_\phi \sim (10^{-17}, 2 \times 10^{-15})$ eV.

VI. SUMMARY

In this paper we compute pulsar periastron advance constraints on ultralight scalar mediators that couple to muons. We consider six pulsar binary systems with precise timing measurements, and find that the PSR J0737-3039A provides the strongest constraint, owing to its highly precise timing measurements. The periastron advance provides the most stringent constraints in the mass range of $m_\phi \in (10^{-17}, 2 \times 10^{-15})$ eV, with the best limit on the scalar muon coupling $g_{\phi\mu} < \mathcal{O}(10^{-21})$ at $m_\phi \simeq 4 \times 10^{-16}$ eV; this surpasses the GW170817 constraints by about an order of magnitude, as shown in Fig. 5.

The pulsar periastron advance constraints on muonic forces are strongly dependent on the muon composition of the neutron stars. We computed the muon fraction of the NSs by using the phenomenologically superior BSk24 EoS [27, 38], which is consistent with both nuclear physics and astrophysical constraints, and is used for analyzing the recently observed binary compact objects merger event GW230529 [35]. Moreover, we consider the effects of the long-range muonic force, which are important when the coupling $g_{\phi\mu}$ is larger than 10^{-19} . The effects of the long-range muonic force become so significant that the muon

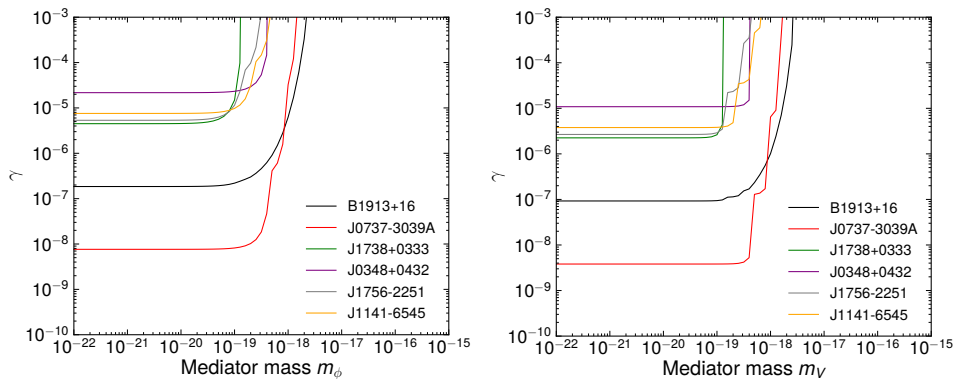


FIG. 4. The 2σ upper bounds on γ from the orbital decay measurements of binary pulsar systems for the scalar (left) and vector (right) cases.

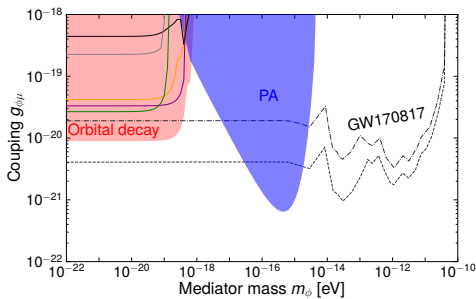


FIG. 5. The 95% CL constraints on the scalar-muon coupling $g_{\phi\mu}$ from the periastron advance (PA) of binary pulsar system PSR J0737-3039 (blue-shaded), and from the orbital decay of binary pulsar systems (red-shaded). Also shown are the GW170817 constraints [10] computed with four different EoSs; the limits with BSk24 lie in between the two extreme cases shown as dashed and dash-dotted curves.

fraction is reduced to one-third of its value in SM when $g_{\phi\mu} \sim 10^{-18}$. We thus conclude that previous studies that neglect the effects of the long-range muonic force overestimate the capability of neutron stars to probe ultralight muonic mediators with large couplings.

In our analysis we also study the constraints on the radiation strength from orbital decay measurements of pulsar-NS and pulsar-WD binaries, for both scalar and vector mediator cases. The latest measurement of PSR J0737-3039A provides the best orbital decay constraints. After taking into account the suppression effects on the muon fraction due to the long-range force, we find that the orbital decay constraints on the scalar coupling $g_{\phi\mu}$ exceed the GW170817 constraints that are calculated under a pessimistic muon fraction assumption [10] for $m_\phi \lesssim 10^{-19}$.

ACKNOWLEDGMENTS

We thank Evan McDonough, Nicolás Yunes, Caroline Owen, and Yiqi Xie for discussions and correspondence.

The work is supported in part by the National Natural Science Foundation of China under Grant No. 12275128.

Appendix A: $npe\mu$ inside neutron star

In this section we present some detailed calculations of NSs, including the nucleon number density $n(r)$, the electron number density $n_e(r)$, the radius of the NS R_{NS} , and the derivation of Eqs. (18-20).

1. Number densities and NS radius

The detailed calculation of the nucleon number density profile $n(r)$ for the BSk24 EoS can be found in Appendix A of Ref. [39]. Below we provide a brief summary of the analysis.

We first obtain the mass-energy density $\rho(r)$ by solving the Tolman-Oppenheimer-Volkoff (TOV) equation [40, 41], together with the EoS BSk24 [27]. This process also yields the mass-radius relation of the NSs, from which we determine the radius for a given NS mass. We then determine the nucleon number density $n(r)$ via [27]

$$\rho(r) = n(r)(e_{\text{eq}} + m_n), \quad (\text{A1})$$

where m_n is the neutron mass, and e_{eq} is the energy per nucleon (without the rest mass term). We obtain the electron number density $n_e(r)$ by using the fitting function $Y_e \equiv n_e(r)/n(r)$, which is given by Eq. (C17) of Ref. [27]. The electron number density $n_e(r)$ is shown in Fig. 2.

2. Chemical potentials at equilibrium

The equilibrium of the $npe\mu$ matter is maintained by the following weak interaction processes: [9]

$$n \rightarrow p + e + \bar{\nu}_e, \quad (\text{A2})$$

$$n \rightarrow p + \mu + \bar{\nu}_\mu, \quad (\text{A3})$$

$$p + e \rightarrow n + \nu_e, \quad (\text{A4})$$

$$p + \mu \rightarrow n + \nu_\mu. \quad (\text{A5})$$

At equilibrium, the chemical potentials on both sides of these interactions are equal, leading to

$$\mu_n = \mu_p + \mu_e, \quad (\text{A6})$$

$$\mu_e = \mu_\mu, \quad (\text{A7})$$

where we have neglected neutrino chemical potentials because the NS core is assumed to be transparent to neutrinos.

3. Lepton chemical potential inside NS

The Fermi distribution of the lepton is given by [42]

$$n_F(E) = \frac{1}{e^{(E-\mu_\ell)/T} + 1}, \quad (\text{A8})$$

where μ_ℓ is the lepton chemical potential.

In the presence of a muonic potential, the energy per lepton inside the NS is

$$E = \sqrt{m_\mu^2 + p^2} + g_{\phi\mu}V, \quad (\text{A9})$$

where p is the momentum of the lepton, and V is the muonic potential. For electrons, $V = 0$.

For a cold NS such that $T \rightarrow 0$, the highest energy level with non-vanishing n_F is $E_{\max} = \mu_\ell$. In this case, the number density of the lepton is given by

$$\begin{aligned} n &= 2 \int \frac{d^3p}{(2\pi)^3} \frac{1}{e^{(E-\mu_\ell)/T} + 1} \\ &= \frac{1}{\pi^2} \int_0^{\sqrt{(\mu_\ell - g_{\phi\mu}V)^2 - m_\ell^2}} dp p^2 \\ &= \frac{1}{3\pi^2} [(\mu_\ell - g_{\phi\mu}V)^2 - m_\ell^2]^{3/2}. \end{aligned} \quad (\text{A10})$$

Inverting Eq. (A10) we find

$$\mu_\ell(r) = \sqrt{m_\ell^2 + [3\pi^2 n_\ell(r)]^{2/3}} + g_{\phi\mu}V(r). \quad (\text{A11})$$

Because the NS radius (~ 10 km) is far smaller than both the semi-major axis ($a \gtrsim 10^6$ km) of the binary systems in our analysis and the mediator wavelength we are interested in, we can approximate the Yukawa potential with the Coulomb potential

$$V(r) = - \int_0^r dr' \frac{Q(r')}{4\pi r'^2}, \quad (\text{A12})$$

where $Q(r')$ is the charge carried by all the muons inside r' :

$$Q(r') = 4\pi g_{\phi\mu} \int_0^{r'} dr'' r''^2 n_\mu(r''). \quad (\text{A13})$$

Appendix B: Pulsar orbital decay

Ultralight mediator can be emitted from the NSs via dipole radiation [36], providing a new energy loss channel beyond the gravitational radiation for binary pulsar systems.

The ratio of the radiation power from new physics to that in GR is [36]⁴

$$\frac{\langle \dot{E} \rangle_{S,V}}{\langle \dot{E} \rangle_G} = \begin{cases} \frac{5}{96} \gamma \left(\frac{P_b}{2\pi GM} \right)^{2/3} \frac{g_S(m_\phi, e)}{g_G(e)} & \text{scalar} \\ \frac{5}{48} \gamma \left(\frac{P_b}{2\pi GM} \right)^{2/3} \frac{g_V(m_V, e)}{g_G(e)} & \text{vector} \end{cases}, \quad (\text{B1})$$

where $g_{S,V}$ are given by

$$\begin{aligned} g_V(m_V, e) &= \sum_{n>n_0} 2n^2 \left[\mathcal{J}_n'^2(ne) + \left(\frac{1-e^2}{e^2} \right) \mathcal{J}_n^2(ne) \right] \\ &\quad \times \sqrt{1 - \left(\frac{n_0}{n} \right)^2} \left[1 + \frac{1}{2} \left(\frac{n_0}{n} \right)^2 \right], \end{aligned} \quad (\text{B2})$$

$$\begin{aligned} g_S(m_\phi, e) &= \sum_{n>n_0} 2n^2 \left[\mathcal{J}_n'^2(ne) + \left(\frac{1-e^2}{e^2} \right) \mathcal{J}_n^2(ne) \right] \\ &\quad \times \left[1 - \left(\frac{n_0}{n} \right)^2 \right]^{3/2}, \end{aligned} \quad (\text{B3})$$

with \mathcal{J}_n being the Bessel function of n -th order, $\mathcal{J}_n'(x) \equiv d\mathcal{J}_n(x)/dx$, and $n_0 \equiv P_b m_{\phi,V}/(2\pi)$. The g_G factor is given by

$$g_G = g_{G,0PN} + g_{G,1PN}, \quad (\text{B4})$$

where $g_{G,0PN}$ and $g_{G,1PN}$ account for the 0PN and 1PN

⁴ Our formulas differ by a factor of $1/4\pi$ from those given in Ref. [36], which uses the Gaussian units.

PSR	$\dot{P}_b^{\text{int}}/\dot{P}_b^{\text{GR}}$	P_b (day)	e	m_1 (M_\odot)	m_2 (M_\odot)
B1916+13 [14]	0.9983 ± 0.0016	0.323	0.617	1.438	1.39
J0737-3039A [13]	0.999963 ± 0.000063	0.102	0.0878	1.338	1.249
*J1738+0333 [43]	0.94 ± 0.13	0.355	$\simeq 3.4 \times 10^{-7}$	1.46	0.181
*J0348+0432 [44]	1.05 ± 0.18	0.102	$\simeq 2 \times 10^{-6}$	2.01	0.172
J1756-2251 [16]	1.08 ± 0.03	0.320	0.181	1.341	1.230
*J1141-6545 [45]	1.04 ± 0.06	0.198	0.172	1.27	1.02

TABLE III. Binary pulsar systems used for the orbital decay constraints. The NS-WD binaries are marked by the “*” symbol.

contributions to the gravitational radiation [30]⁵

$$g_{G,0\text{PN}} = \frac{1 + \frac{73}{24}e^2 + \frac{37}{96}e^4}{(1 - e^2)^{7/2}}, \quad (\text{B5})$$

$$g_{G,1\text{PN}} = \frac{10k}{3}g_{G,0\text{PN}} + \left(\frac{P_b}{2\pi GM}\right)^{-2/3} \frac{1}{(1 - e^2)^{9/2}} \\ \times \left[-\frac{1247}{336} - \frac{35}{12}\eta + e^2 \left(\frac{10475}{672} - \frac{1081}{36}\eta\right) \right. \\ \left. + e^4 \left(\frac{10043}{384} - \frac{311}{12}\eta\right) + e^6 \left(\frac{2179}{1792} - \frac{851}{576}\eta\right) \right], \quad (\text{B6})$$

where $k = 3(P_b/2\pi GM)^{-2/3}(1 - e^2)^{-1}$, and $\eta =$

$$m_1 m_2 / (m_1 + m_2)^2.$$

Table III shows the binary pulsar systems used to calculate the orbital decay constraints. For each binary system, we provide the ratio of its intrinsic orbital decay to that predicted by GR, along with other relevant parameters. Note that the orbital decay ratio of PSR J0737-3039A, as given by Ref. [13], accounts for higher-order effects not included in other binary pulsar systems. These include (i) the 1PN contribution to the GW radiation in computing \dot{P}_b^{GR} , and (ii) the mass loss effect in calculating \dot{P}_b^{int} .⁶ Both effects are smaller than the uncertainty of \dot{P}_b^{int} .

-
- [1] C. M. Will, “The Confrontation between General Relativity and Experiment,” *Living Rev. Rel.* **17** (2014) 4 [arXiv:1403.7377].
- [2] G. M. Tino, L. Cacciapuoti, S. Capozziello, G. Lambiase, and F. Sorrentino, “Precision Gravity Tests and the Einstein Equivalence Principle,” *Prog. Part. Nucl. Phys.* **112** (2020) 103772 [arXiv:2002.02907].
- [3] E. G. Adelberger, *et al.*, “Particle Physics Implications of a Recent Test of the Gravitational Inverse Square Law,” *Phys. Rev. Lett.* **98** (2007) 131104 [hep-ph/0611223].
- [4] S. Schlamminger, K. Y. Choi, T. A. Wagner, J. H. Gundlach, and E. G. Adelberger, “Test of the equivalence principle using a rotating torsion balance,” *Phys. Rev. Lett.* **100** (2008) 041101 [arXiv:0712.0607].
- [5] T. A. Wagner, S. Schlamminger, J. H. Gundlach, and E. G. Adelberger, “Torsion-balance tests of the weak equivalence principle,” *Class. Quant. Grav.* **29** (2012) 184002 [arXiv:1207.2442].
- [6] J. Bergé, *et al.*, “MICROSCOPE Mission: First Constraints on the Violation of the Weak Equivalence Principle by a Light Scalar Dilaton,” *Phys. Rev. Lett.* **120** (2018) 141101 [arXiv:1712.00483].
- [7] J. G. Williams, S. G. Turyshev, and D. H. Boggs, “Progress in lunar laser ranging tests of relativistic gravity,” *Phys. Rev. Lett.* **93** (2004) 261101 [gr-qc/0411113].
- [8] S. G. Turyshev and J. G. Williams, “Space-based tests of gravity with laser ranging,” *Int. J. Mod. Phys. D* **16** (2007) 2165–2179 [gr-qc/0611095].
- [9] P. Haensel, A. Y. Potekhin, and D. G. Yakovlev, *Neutron stars 1: Equation of state and structure*, vol. 326. Springer, New York, USA, 2007.
- [10] J. A. Dror, R. Laha, and T. Opferkuch, “Probing muonic forces with neutron star binaries,” *Phys. Rev. D* **102** (2020) 023005 [arXiv:1909.12845].
- [11] X.-J. Xu, “The ν_R -philic scalar: its loop-induced interactions and Yukawa forces in LIGO observations,” *JHEP* **09** (2020) 105 [arXiv:2007.01893].
- [12] T. Kumar Poddar, S. Mohanty, and S. Jana, “Vector gauge boson radiation from compact binary systems in a gauged $L_\mu - L_\tau$ scenario,” *Phys. Rev. D* **100** (2019) 123023 [arXiv:1908.09732].
- [13] M. Kramer *et al.*, “Strong-Field Gravity Tests with the Double Pulsar,” *Phys. Rev. X* **11** (2021) 041050 [arXiv:2112.06795].
- [14] J. M. Weisberg and Y. Huang, “Relativistic

⁵ As shown in equation (547) of Ref. [30], the 0PN contribution to GW radiation includes a factor of x^5 , where $x = (P_b/2\pi GMK)^{-2/3}$ with $K = 1 + k = 1 + \Delta\omega/2\pi$ being the number of orbits the pulsar completes in one period. Expanding x^5 in terms of k results in the first term in the expression for $g_{G,1\text{PN}}$, which is of the 1PN order, as given in Eq. (B6).

⁶ The intrinsic orbital decay after removing the mass loss effect is denoted as \dot{P}_b^{GR} in Ref. [13]. For simplicity, we still denote it as \dot{P}_b^{int} here.

- Measurements from Timing the Binary Pulsar PSR B1913+16,” *Astrophys. J.* **829** (2016) 55 [arXiv:1606.02744].
- [15] J. van Leeuwen *et al.*, “The Binary Companion of Young, Relativistic Pulsar J1906+0746,” *Astrophys. J.* **798** (2015) 118 [arXiv:1411.1518].
- [16] R. D. Ferdman *et al.*, “PSR J1756–2251: a pulsar with a low-mass neutron star companion,” *Mon. Not. Roy. Astron. Soc.* **443** (2014) 2183–2196 [arXiv:1406.5507].
- [17] B. A. Jacoby, *et al.*, “Measurement of Orbital Decay in the Double Neutron Star Binary PSR B2127+11C,” *Astrophys. J. Lett.* **644** (2006) L113–L116 [astro-ph/0605375].
- [18] E. Fonseca, I. H. Stairs, and S. E. Thorsett, “A Comprehensive Study of Relativistic Gravity using PSR B1534+12,” *Astrophys. J.* **787** (2014) 82 [arXiv:1402.4836].
- [19] I. H. Stairs, “Testing general relativity with pulsar timing,” *Living Rev. Rel.* **6** (2003) 5 [astro-ph/0307536].
- [20] N. Wex, “Testing Relativistic Gravity with Radio Pulsars.” arXiv:1402.5594.
- [21] E. Berti *et al.*, “Testing General Relativity with Present and Future Astrophysical Observations,” *Class. Quant. Grav.* **32** (2015) 243001 [arXiv:1501.07274].
- [22] P. C. C. Freire and N. Wex, “Gravity experiments with radio pulsars,” *Living Rev. Rel.* **27** (2024) 5 [arXiv:2407.16540].
- [23] D. Blas, D. López Nacir, and S. Sibiryakov, “Secular effects of ultralight dark matter on binary pulsars,” *Phys. Rev. D* **101** (2020) 063016 [arXiv:1910.08544].
- [24] P. Kūš, D. López Nacir, and F. R. Urban, “Bayesian sensitivity of binary pulsars to ultra-light dark matter.” arXiv:2402.04099.
- [25] M. Fabbrichesi and A. Urbano, “Charged neutron stars and observational tests of a dark force weaker than gravity,” *JCAP* **06** (2020) 007 [arXiv:1902.07914].
- [26] **LIGO Scientific, Virgo** Collaboration, “GW170817: Observation of Gravitational Waves from a Binary Neutron Star Inspiral,” *Phys. Rev. Lett.* **119** (2017) 161101 [arXiv:1710.05832].
- [27] J. M. Pearson, *et al.*, “Unified equations of state for cold non-accreting neutron stars with Brussels–Montreal functionals – I. Role of symmetry energy,” *Mon. Not. Roy. Astron. Soc.* **481** (2018) 2994–3026 [arXiv:1903.04981]. [Erratum: *Mon. Not. Roy. Astron. Soc.* 486, 768 (2019)].
- [28] R. A. Hulse and J. H. Taylor, “Discovery of a pulsar in a binary system,” *Astrophys. J. Lett.* **195** (1975) L51–L53.
- [29] E. Poisson and C. M. Will, *Gravity: Newtonian, Post-Newtonian, Relativistic*. Cambridge University Press, 2014.
- [30] L. Blanchet, “Gravitational Radiation from Post-Newtonian Sources and Inspiralling Compact Binaries,” *Living Rev. Rel.* **17** (2014) 2 [arXiv:1310.1528].
- [31] C. M. Will, *Theory and Experiment in Gravitational Physics*. Cambridge University Press, 2018.
- [32] T. Damour and G. Schaefer, “Higher Order Relativistic Periastron Advances and Binary Pulsars,” *Nuovo Cim. B* **101** (1988) 127.
- [33] T. Damour and N. Deruelle, “General relativistic celestial mechanics of binary systems. II. The post-newtonian timing formula,” *Annales de l’I. H. P. Physique théorique* **44** (1986) 263–292.
- [34] T. Damour and J. H. Taylor, “Strong field tests of relativistic gravity and binary pulsars,” *Phys. Rev. D* **45** (1992) 1840–1868.
- [35] **LIGO Scientific, Virgo,, KAGRA, VIRGO** Collaboration, “Observation of Gravitational Waves from the Coalescence of a 2.5–4.5 M_{\odot} Compact Object and a Neutron Star,” *Astrophys. J. Lett.* **970** (2024) L34 [arXiv:2404.04248].
- [36] D. Krause, H. T. Kloor, and E. Fischbach, “Multipole radiation from massive fields: Application to binary pulsar systems,” *Phys. Rev. D* **49** (1994) 6892–6906.
- [37] S. L. Shapiro and S. A. Teukolsky, *Black holes, white dwarfs, and neutron stars: The physics of compact objects*. 1983.
- [38] J. M. Pearson, N. Chamel, and A. Y. Potekhin, “Unified equations of state for cold nonaccreting neutron stars with Brussels–Montreal functionals. II. Pasta phases in semiclassical approximation,” *Phys. Rev. C* **101** (2020) 015802 [arXiv:2001.03876].
- [39] Z. Liu and Z.-W. Tang, “Probing ultralight isospin-violating mediators at GW170817.” arXiv:2402.06209.
- [40] R. C. Tolman, “Static solutions of Einstein’s field equations for spheres of fluid,” *Phys. Rev.* **55** (1939) 364–373.
- [41] J. R. Oppenheimer and G. M. Volkoff, “On massive neutron cores,” *Phys. Rev.* **55** (1939) 374–381.
- [42] C. Kittel and H. Kroemer, *Thermal Physics*. W. H. Freeman, 1980.
- [43] P. C. C. Freire, *et al.*, “The relativistic pulsar-white dwarf binary PSR J1738+0333 II. The most stringent test of scalar-tensor gravity,” *Mon. Not. Roy. Astron. Soc.* **423** (2012) 3328 [arXiv:1205.1450].
- [44] J. Antoniadis *et al.*, “A Massive Pulsar in a Compact Relativistic Binary,” *Science* **340** (2013) 6131 [arXiv:1304.6875].
- [45] N. D. R. Bhat, M. Bailes, and J. P. W. Verbiest, “Gravitational-radiation losses from the pulsar-white-dwarf binary PSR J1141–6545,” *Phys. Rev. D* **77** (2008) 124017 [arXiv:0804.0956].